Modelling of Low Velocity Impact Damage in Laminated Composites

Jounghwan Lee
Researcher, Graduate School of Aerospace Engineering, The University of Sheffield, U.K.
Changduk Kong*
Professor, Department of Aerospace Engineering, Chosun University, Kwangju 501-759, Korea
Costas Soutis
Professor, Aerospace Engineering, The University of Sheffield, U.K.

In this study a simple model is developed that predicts impact damage in a composite laminate avoiding the need of the time-consuming dynamic finite element method (FEM). The analytical model uses a non-linear approximation method (Rayleigh-Ritz) and the large deflection plate theory to predict the number of failed plies and damage area in a quasi-isotropic composite circular plate (axisymmetric problem) due to a point impact load at its centre. It is assumed that the deformation due to a static transverse load is similar to that oc curred in a low velocity impact. It is found that the model, despite its simplicity, is in good agreement with FEM predictions and experimental data for the deflection of the composite plate and gives a good estimate of the number of failed plies due to fibre breakage. The predicted damage zone could be used with a fracture mechanics model developed by the second investigator and co-workers to calculate the compression after impact strength of such laminates. This approach could save significant running time when compared to FEM solutions.

Key Words: Low Velocity Impact Model, Non-linear Approximation Method, Composite Laminate, Compression After Impact Strength

1. Introduction

The damage caused to carbon fibre composite structures by low velocity impact, and the resulting reduction in compression after impact (CAI) strength has been well known for many years (Whitehead, 1985; Geszczuk, 1982) and is of particular concern to the aerospace industry, both military and civil.

An impact damage site in a composite laminate contains delaminations, matrix cracking and fibre fracture (Kim, 2003). A model to predict the damage area taking into account all these factors is complex and could take considerable time and funding to develop. The problem could be simplified by making some assumptions about the nature of the impact damage. Several methods (Liu, 1988; Fuoss, 1994, 1998; Murri, 1988; Suemasu, 1996, 1998) have been developed based on the concept of mismatch of bending stiffness, energy release rate and bending strain and use a parameter that is directly related to the damage state. This damage parameter can be calculated using measurable data from the impact event and/or material and geometric properties of the laminate. Predicting damage using such a parameter can be suitable for preliminary design analysis, as the calculation time could be con-

* Corresponding Author,
E-mail: cdgong@mail.chosun.ac.kr
TEL: +82-62-230-7188; **FAX**: +82-62-230-7188
Professor, Department of Aerospace Engineering, Chosun University, 375 Seosuk-dong, Dong-gu, Gwangju 501-759, Korea. (Manuscript **Received** November 29, 2004; **Revised** December 15, 2004)

siderably shorter than 3-D detailed FE modelling. Most of these models have mainly focused on predicting delamination and matrix cracking due to low velocity impact but few have dealt with fibre breakage.

The aim of this work is to develop an impact damage model for preliminary design analysis that avoids the need of a dynamic finite element analysis of the structure. The model only deals with fibre breakage mode for impacted laminate plates. In this work a simple non-linear approximation method (Rayleigh-Ritz method) is followed to predict the impact damage size due to fibre breakage. This result could then be used as basic input data for predicting the compressive after impact (CAI) strength with the Soutis-Fleck model (Soutis, 1990). A commercial programme, Maple VI is used to run the present model and FE analysis together with experimental data to evaluate its accuracy.

2. Impact Damage Modelling

The impact damage model is based on the concept that the low velocity impact response is similar to the deformation due to a static concentrated lateral load (Sjobolm, 1988) and that when a plate is subjected to such a lateral loading, the expressions for the deflection of both isotropic and composite plates have the same form (Lee and Sun, 1995). In the model, by neglecting the inertia forces of the plate, the problem is reduced to a static equivalent one. By considering degraded stiffness in the plate with increasing loads, idealized damage accumulation is modelled using the Rayleigh-Ritz method together with the principle of virtual displacement (PVD). In addition, energy is correlated to force and deformation by considering the load-deflection relationship and assuming that the maximum strains occur at the maximum deflection when all impact kinetic energy has been absorbed by elastic deformation and damage.

Let us consider a clamped circular plate as shown in Fig. 1. Transverse point load P is applied at its centre. The plate is divided into R_N regions, which have different degraded stiffness at each region, due to fibre damage. Deflection is finite and geometrical nonlinearity is considered. In order to simplify the problem further, the following assumptions are introduced. Through-thickness shear flexibility and in-plane displacements are neglected. The plate has an axisymmetric deformation through thickness. Kirchhoff's hypothesis is assumed to be valid even in the neighbourhood of the fibre damage edges. Also, in order to determine fibre damage of radius r for a quasi-isotropic plate, it is assumed that the maximum failure strain (ε_{11}) along the fibre direction can be used as a damage criterion. Then by assuming axisymmetric deformation, we make this criterion fit for all radial strain (ε_r). However the plate is only quasi isotropic so this is an approximation for bending strains. For mem-

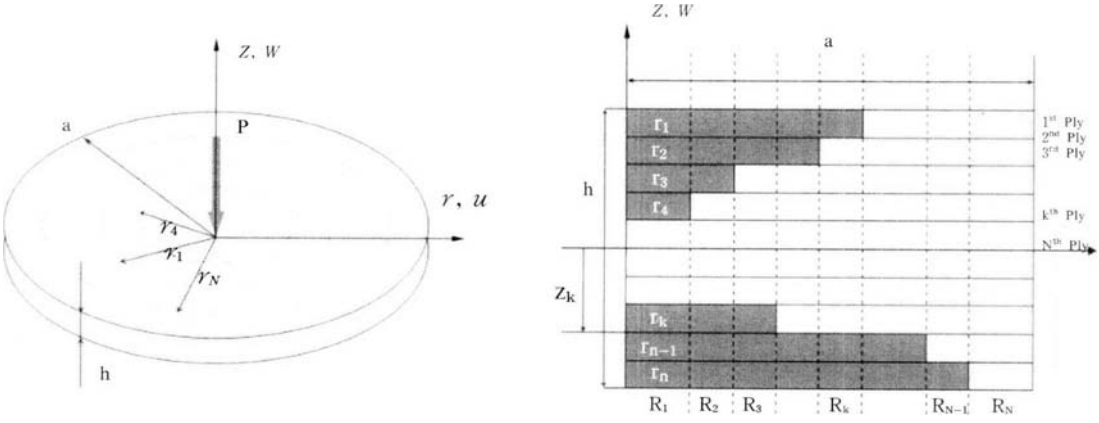

Fig. 1 Circular plate with fibre damage radius r_1, r_2, r_K, $\cdots$, and r_N at each ply

brane strains, uniform through thickness, we can use this criterion for ε_{11} knowing that it is also true for (ε_{22}) and (ε_{45°).

The clamped boundary condition has been chosen since we are modelling a local impact zone, the edge of which will be tangential to the global displacement. The boundary conditions at the plate boundary $r=a$ and the plate centre $r=0$ are written as

$$w_{r=a}=\frac{dw_{r=0}}{dr}=\frac{dw_{r=a}}{dr}=0 \tag{1}$$

where $w_{r=0}$ and $w_{r=a}$ denote the transverse displacements of the undamaged plate at its centre and boundary edge, respectively. Owing to the Kirchhoff's hypothesis, the continuity conditions of displacements at the fibre damage edge r_1, r_2, r_K, $\cdots$, and r_N of each ply are simply written as

$$\begin{aligned} {w_0}^{r_1}&={w_d}^{r_1},\quad \frac{d{w_0}^{r_1}}{dr}=\frac{d{w_d}^{r_1}}{dr}\\ {w_0}^{r_2}&={w_d}^{r_2},\quad \frac{d{w_0}^{r_2}}{dr}=\frac{d{w_d}^{r_2}}{dr}\\ {w_0}^{r_k}&={w_d}^{r_k},\quad \frac{d{w_0}^{r_k}}{dr}=\frac{d{w_d}^{r_k}}{dr} \end{aligned} \tag{2}$$

where ${w_0}^{r_k}$ and ${w_d}^{r_k}$ are the transverse displacements of the undamaged and the damaged portion at the k^{th} ply, respectively. In Fig. 1, R_1 to R_N denote the regions, which have a different stiffness. Z_k is a distance of the bottom surface of the k^{th} ply measured from the middle plane of the plate.

When deriving the elastic energy expressions and dealing with fibre damage areas that are circular in shape, it is convenient to describe their geometry in terms of polar co-ordinates (Timoshenko, 1959). Membrane stretching energy (U_S) and bending energy (U_B) per unit area in the polar co-ordinate system are:

$$\begin{aligned} U_S=\frac{1}{8}\Big[&A_{11}\Big(\frac{\partial w}{\partial r}\Big)^4\cos^4\theta+A_{22}\Big(\frac{\partial w}{\partial r}\Big)^4\sin^4\theta\\ &+2(A_{12}+A_{66})\Big(\frac{\partial w}{\partial r}\Big)^4\sin^2\theta\cos^2\theta\Big] \end{aligned} \tag{3}$$

$$U_B=J\cos^4\theta+K\sin^4\theta+L\sin^2\theta \tag{4}$$

where A_{ij} is the laminate extensional stiffness matrix. Parameters J, K and L are as follows:

$$J=\frac{1}{2}\Big(\Big(\frac{\partial^2 w}{\partial r^2}\Big)^2D_{11}+\frac{2}{r}\frac{\partial^2 w}{\partial r^2}\frac{\partial w}{\partial r}D_{12}+\frac{1}{r^2}\Big(\frac{\partial w}{\partial r}\Big)^2D_{22}\Big) \tag{5}$$

$$K=\frac{1}{2}\Big(\Big(\frac{\partial^2 w}{\partial r^2}\Big)^2D_{22}+\frac{2}{r}\frac{\partial^2 w}{\partial r^2}\frac{\partial w}{\partial r}D_{12}+\frac{1}{r^2}\Big(\frac{\partial w}{\partial r}\Big)^2D_{11}\Big) \tag{6}$$

$$\begin{aligned} L=\frac{1}{2}\Big(&\Big(\frac{\partial^2 w}{\partial r^2}\Big)^2(D_{12}+D_{66})+\frac{1}{r}\frac{\partial^2 w}{\partial r^2}\frac{\partial w}{\partial r}\\ &\times(D_{11}+D_{22}-2D_{66})+\frac{1}{r^2}\Big(\frac{\partial w}{\partial r}\Big)^2(D_{12}+D_{66})\Big) \end{aligned} \tag{7}$$

where D_{ij} is the laminate bending stiffness.

The total membrane stretching and bending energy of a circular plate of radius a is obtained by integrating over the area of the plate. The total internal energy is obtained by adding the total bending energy equation to the total membrane stretching energy equation. Thus, the total energy U_T is expressed as

$$\begin{aligned} U_T=\int_0^a\Big(&A\Big(\Big(\frac{d^2w}{dr^2}\Big)^2+\Big(\frac{1}{r^2}\frac{dw}{dr}\Big)^2\Big)\\ &+B\Big(\frac{1}{r}\frac{d^2w}{dr^2}\frac{dw}{dr}\Big)+C\Big(\frac{dw}{dr}\Big)^4r\,dr\Big) \end{aligned} \tag{8}$$

where

$$A=\frac{\pi}{8}(3D_{11}+3D_{22}+2D_{12}+4D_{66})$$

$$B=\frac{\pi}{4}(D_{11}+D_{22}+6D_{12}-2D_{66})$$

and

$$C=\frac{\pi}{32}(3A_{11}+3A_{22}+2A_{12}+4A_{66})$$

The work W done by the external force P is simply given as a product of force and displacement where the point load is applied.

$$W=Pw(0) \tag{9}$$

In order to obtain the transverse displacement w, the Rayleigh-Ritz method applied to PVD (the principle of virtual displacement) is adopted to have an approximated solution. The displacement function for fully clamped boundary conditions is assumed as (Timoshenko, 1959)

$$w=w_0\Big(1-\frac{r^2}{a^2}+2\frac{r^2}{a^2}\log\frac{r}{a}\Big) \tag{10}$$

This function satisfies the boundary condition Eq. (1) as an admissible function. When equating the total internal energy Eq. (8) to the external

energy Eq. (9) (Equilibrium State $U_T - W = 0$), we can produce a general equation obtained for predicting the finite transverse displacement as follows:

$$\int_0^a \left(A\left(\left(\frac{d^2w}{dr^2} \right)^2 + \left(\frac{1}{r^2} \frac{dw}{dr} \right)^2 \right) + B\left(\frac{1}{r} \frac{d^2w}{dr^2} \frac{dw}{dr} \right) + C\left(\frac{dw}{dr} \right)^4 \right) r dr - Pw(0) = 0 \tag{11}$$

Substituting displacement function Eq. (10) into Eq. (11), the total internal energy and external work using PVD are finally expressed in terms of virtual displacement $\bar{w}_0$ as:

$$U_T - W = \left(A\frac{16}{a^2} w_0 + C\frac{256}{81a^2} w_0^3 \right) \bar{w}_0 - P\bar{w}_0 = 0$$
$$\Rightarrow C\frac{256}{81a^2} w_0^3 + A\frac{16}{a^2}{}_0 - P = 0 \tag{12}$$

where P is the point load at the centre of the circular plate and w_0 is the displacement at $r = 0$.

The root of Eq. (12) gives the displacement of the elastic circular plate at its centre and when is inserted into displacement function Eq. (10), the displacement at any point along the radial direction r is derived. In order to solve for w_0, the program 'Maple VI' is used (Monagan, 2000).

2.1 Prediction of impact damage

In order to predict damage area, the maximum failure strain criterion is adopted. For simplicity, it is assumed that ply damage occurs if any radial strain value (ε_r) along the radius r exceeds its ultimate mean strain between tensile strain value (ε_{11}^T) and compressive strain value (ε_{11}^C). It is also assumed that the ply damage has a circular shape of radius r due to the axisymmetric out-of-plane displacement field. The maximum strain criterion is formulated below:

$$\frac{\varepsilon_r}{\varepsilon_{11}^{T/C}} \geq 1 \tag{13}$$

where ε_r denotes radial strain at each ply and $\varepsilon_{11}^{T/C}$ is the ultimate mean strain between unidirectional tensile and compressive failure strain.

In the non-linear case, the k^{th} ply radial strain equation is expressed as the combination of membrane stretching radial strain and bending radial strain, i.e.,

$$\varepsilon_r^k = \varepsilon_{Sr} + \varepsilon_{Br} = \frac{1}{2}\left(\frac{dw}{dr} \right)^2 + Z_k\left(\frac{d^2w}{dr^2} \right) \tag{14}$$

where ε_{Sr} is the membrane stretching radial strain and ε_{Br} is the bending radial stain. Z_k is a distance of the bottom surface of the k^{th} ply measured from the plate's middle plane, Fig. 1(b).

2.2 Damage accumulation process

Strategy for damage accumulation is based on the degraded stiffness region of the circular plate, as shown in Fig. 1(b). When a certain load is applied to the plate, the extent of damage i.e. r_1, r_2, r_3, $\cdots$, and r_N at each ply is determined using the maximum strain criterion Eq. (13) and also number of failed plies. Based on these failed plies, the plate is divided into N regions, which have a different degraded membrane and bending stiffnesses, see Fig. 1(b). Thus, in Fig. 1(b), region R_1 shows the most degraded stiffness region and region R_N represents the undamaged region. Considering Kirchhoff's hypothesis, which is the continuity condition of displacement at the damage edge, the total strain energy Eq. (8) is expressed as follows:

$$\begin{aligned} U_T = & \int_0^{r_4} \left(A_1\left((w'')^2 + \left(\frac{1}{r^2} w' \right)^2 \right) + B_1 \frac{1}{r} w'' w' + C_2 w'^4 \right) r dr \\ & + \int_{r_4}^{r_3} \left(A_2\left((w'')^2 + \left(\frac{1}{r^2} w' \right)^2 \right) + B_2 \frac{1}{r} w'' w' + C_2 w'^4 \right) r dr + \cdots \\ & + \int_{r_3}^{r_1} \left(A_k\left((w'')^2 + \left(\frac{1}{r^2} w' \right)^2 \right) + B_k \frac{1}{r} w'' w' + C_k w'^4 \right) r dr + \cdots \\ & + \int_{r_1}^{a} \left(A_N\left((w'')^2 + \left(\frac{1}{r^2} w' \right)^2 \right) + B_N \frac{1}{r} w'' w' + C_N w'^4 \right) r dr \end{aligned} \tag{15}$$

where A_1, B_1 and C_1 are degraded membrane and bending stiffness deduced from Eq. (8) at region R_1 which is situated between 0 and r_4 along radius r, see Fig. 1(b). A_1, B_2 and C_2 are degraded membrane and bending stiffness parameters deduced from Eq. (8) at region R_2, which is situated between r_4 and r_3 along radius r. A_k, B_k and C_k are degraded membrane and bending stiffnesses estimated by Eq. (8) at region R_k, which is situated between r_2 and r_1 along radius r. A_N, B_N and C_N are same as elastic membrane and bending stiffnesses of Eq. (8) at region R_N, which is situated between r_1 and plate radius, a, along radius r because there are no failed plies. In

order to calculate the degraded membrane and bending stiffnesses, the material properties of the failed plies at each region are eliminated using the classical laminate plate theory.

The above Eq. (15) expresses the degraded internal strain energy of the damaged plate at a certain applied load. Again, equating Eq. (15) to the external work Eq. (9) and calculating the equations like in the elastic plate case, the degraded plate deflection and the propagated damage area are obtained. This procedure is repeated in a piece-wise non-linear iteration procedure beyond initial damage. Finally, impact energy is correlated to force and deformation by considering the load-deflection relationship of the damaged plate.

3. Model Set-up for Validation

3.1 Finite element modelling for nonlinear static and dynamic analysis

A finite element analysis was used to examine the accuracy of the present analysis for the transverse displacement of an elastic circular plate for various values of applied load P. The material modelled was an IM7/8552 multidirectional 3 mm thick carbon fibre composite circular plate with lay-up $[45/-45/90/0]_{3s}$. The through-thickness (Z-direction) displacements were calculated using FE77 (Hitchings, 1995).

A two-dimensional nonlinear static and dynamic finite element analysis were performed. A uniformly distributed load of 12KN on a circular area (diameter : 12 mm) for the nonlinear static analysis is applied at the centre of the circular plate (plate diameter : 102 mm) and the plate is fully clamped at the plate edge. The diameters for the loading area and the circular plate are the same as those used in the experimental test. In this approach, surface quadrilateral 8-node elements were used for nonlinear static and dynamic analyses with 396 elements. A typical finite element mesh for both analyses is illustrated in Fig. 2.

In the dynamic analysis, the impactor is modelled as a lumped mass and interacts with the centre of a target plate with the contact deformation governed by the well-known nonlinear

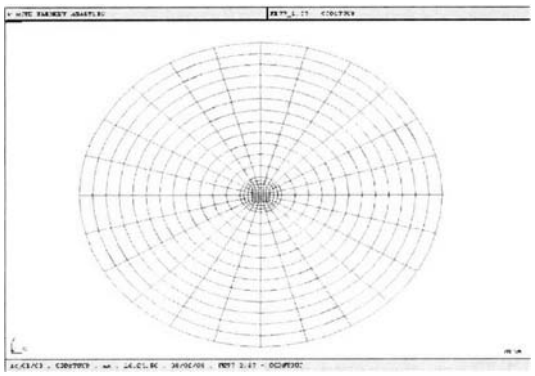

Fig. 2 Finite element mesh for nonlinear static and dynamic analysis of the circular plate

Hertzian contact laws (Khoo, 1991 ; Watson 1994). For the present model, the constants for indentation laws used for carbon/epoxy plate fully clamped in Ref. 15 were applied. They are $k=1.413\times10^{6}$ N/cm$^{1.5}$, $n=1.5$, $q=2.5$, $\beta=0.094$ and $\alpha_p=1.667\times10^{\square 2}$ cm (n, q, β are dimensionless).

In order to compare fibre damage development calculated by the present model using the damage accumulation process, the progressive failure analysis proposed by Chang (Chang, 1987) within FE77 was used.

3.2 Damage prediction model

Fibre damage modelling at ply level in 1 mm and 3 mm thick composite circular plates (Cytec Fiberite IM7/8552) was performed. The plates were 102 mm in diameter, fully clamped and the material properties and stacking sequences are given below :

Material Properties :

$$E_{11}=155\text{ GPa},\ E_{22}=10\text{ GPa}$$
$$\nu_{12}=0.31,\ G_{12}=4.5\text{ Gpa}$$

Ultimate tensile failure strain, $\varepsilon_{11}^{T}=1.54\%$

Ultimate compressive failure strain, $\varepsilon_{11}^{C}=1.1\%$

Stacking Sequences :

$[45/-45/0/90]_s$ and $[45/-45/0/90]_{3s}$

It is assumed that the first ply (top ply) has already failed due to the contact force of the impactor. The damaged region is regarded as being equivalent to the impactor radius, 6 mm.

Estimated radial tensile and compressive strains (ε_r) are compared to the failure value of ε_{11}^T and ε_{11}^C, respectively for determining the extent of the fibre damage at each ply.

4. Results

The theoretical results for undamaged plate deflection, strains, damage area and damaged plate deflection predicted from the present model and FE77 are compared with the experimental results (Lee, 2003) measured from quasi-static and impact tests for a 3 mm thick IM7/8552 $[45/-45/0/90]_{3s}$ carbon fibre composite circular plate. (See Ref. Lee, 2003 for 1 mm thick IM7/8552 $[45/-45/0/90]_s$ experimental and numerical results).

For the nonlinear dynamic analysis (FE77), the laminate is impacted by a 5.52 kg impactor at a velocity of 2.5 m/s, generating an impact energy of 17.8 J. Also, for the nonlinear dynamic progressive failure analysis, the laminate is loaded with the same impact mass at different velocities, generating impact energy levels of between 5 and 60 J.

Only two sets of impact tests were performed with different impactor masses due to the limitation of test coupons. Firstly, 3 mm thick IM7/8552, $[45/-45/0/90]_{3s}$, circular plates were subjected to low-velocity impacts (5 to 11 J) with an impactor mass of 1.58 kg. Then, impact tests were carried out with a 5.52 kg impactor mass resulting in incident energies between 16−19 J.

4.1 Un-degraded deflection comparison between model, FE and experimental results

In Fig. 3 comparisons of theoretical and experimental force-displacement results are shown; the displacement is measured at the centre of the plate. The predictions from the approximate solution (present model) and numerical solution for nonlinear static and dynamic analysis (FE77) are in excellent agreement. There is, however, small discrepancy between predictions and measurements in the figure. This might be caused by a difference between the boundary condition prescribed in the theoretical simulation and that realized in the experiment.

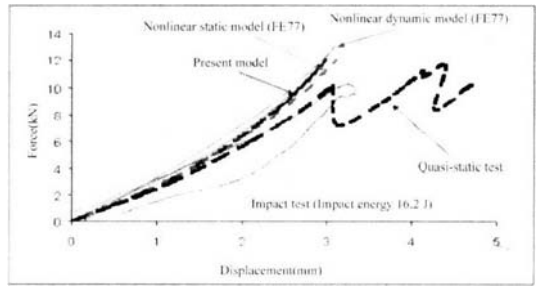

Fig. 3 Force-central deflection curves for a 3 mm thick IM7/8552 $[45/-45/0/90]_{3s}$ circular plate

For a clamped laminate, in the theoretical calculation, the boundaries are strictly restrained from translation and rotation. However, in the experiment, it is not possible to completely prevent the laminate edges from some movement. Thus, the theoretical analysis tends to provide an over-estimated flexural stiffness compared to the experiment, hence resulting in a higher peak force (Davies, 1995; Liou, 1996).

The CPU time spent on the static analysis by using the present model is reduced immensely, producing an accurate prediction for the maximum impact force and deflection when compared with the dynamic finite element computation. For this laminate, the CPU time for the static analysis is only five seconds compared to 2460 minutes for the dynamic FE computation.

4.2 Strain comparison between model and experimental results

Figures 4(a) and (b) show the analytical and measured static bending strains at the top and bottom surface of a 3 mm thick IM7/8552 $[45/-45/0/90]_{3s}$ circular plate. Strain gauges were attached on the top surface at 10 mm and 20 mm away from the centre and the bottom face, at the centre and 20 mm away.

In the present model, the nonlinear bending strains were calculated from Eq. (14) that accounts for membrane stretching and bending strains. Tensile strain is measured and predicted at 20 mm away from centre of the top surface.

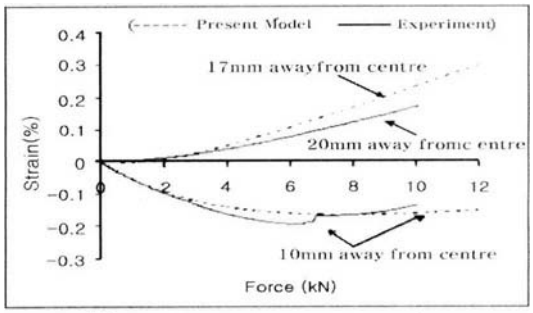

(a) Bending strain at the top surface

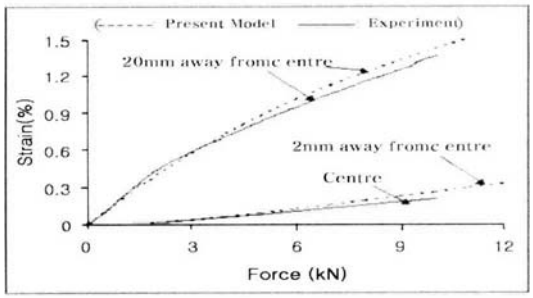

(b) Bending strain at the bottom surface

Fig. 4 Comparison between predicted and measured strains : (a) at the top surface and (b) bottom surface of a 3 mm thick IM7/8552 $[45/-45/0/90]_{3s}$ circular plate

This is caused by the membrane stretching effect away from the centre of the top surface. In general the analytical and experimental strains are in good agreement.

4.3 Damage area predictions in a 3 mm thick circular plate

For the prediction of the damage area a property degradation model needs to be adopted. In the present analysis, it is assumed that the overall elastic properties (E_{11} and E_{22}, G_{12} and ν_{12}) of the damaged region in each failed ply are zero. It is also assumed that the properties of the undamaged area of the failed ply are reduced to $0.5\times E_{11}$ and $0.1\times(E_{22}$, G_{12} and $\nu_{12})$ due to stiffness caused by the fibre breakage in the neighbouring region. The reduced overall elastic moduli of the damaged region in the plate are estimated by the classical laminate plate theory.

In this damage analysis the maximum applied load is 18 kN and it is increased by 1 kN increments with each iteration. Fibre damage is

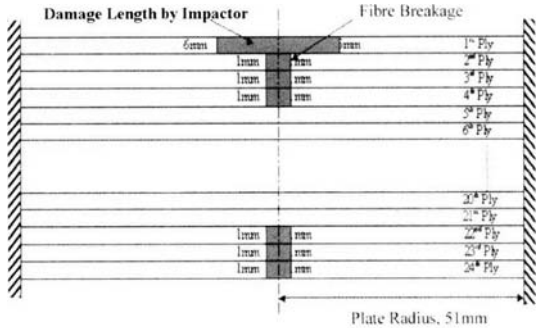

(a) Through-thickness fibre damage, applied load 7 kN

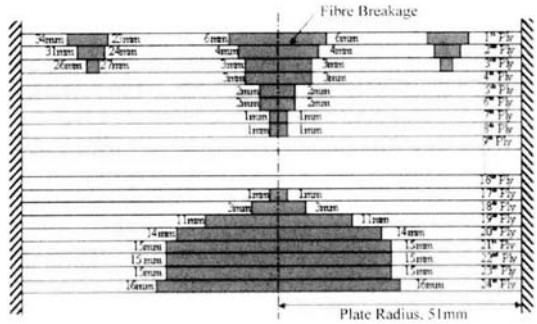

(b) Through-thickness fibre damage, applied load 18 kN

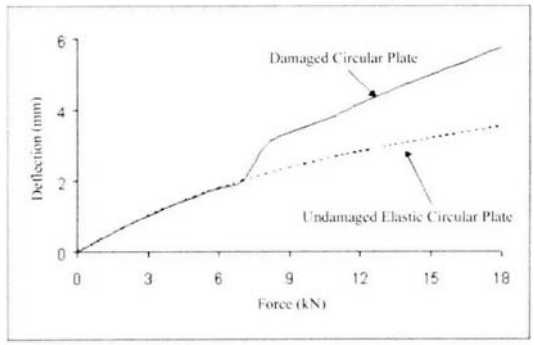

(c) Central deflection versus applied force

Fig. 5 Through-thickness (Z-r plane) fibre damage in a 3 mm thick $[45/-45/0/90]_{3s}$ circular plate

initiated at the plate centre at an applied load of 7 kN and propagates to the plate edge with increasing load. Damage is found in plies 1 (loaded top ply), 2, 3, 4, 22, 23 and 24 (See Fig. 5 (a)). The central deflection of the degraded plate is 2.616 mm and the reduced stiffness properties calculated by the laminate plate theory are: E_x=39.7 GPa, E_y=42.6 GPa, G_{xy}=15.2 GPa,

ν_{xy}=0.29 and ν_{yx}=0.31. At an applied load of 18 kN, the central deflection of the degraded plate is 5.77 mm and the reduced stiffness properties are: E_x= 19.8 GPa, E_y=19.8 GPa, G_{xy}=7.5 GPa, ν_{xy}=0.31 and ν_{yx}=0.31.

Figure 5(a) and (b) illustrate fibre breakage at each ply for an applied load of 7 kN and 18 kN. Respectively. With increasing applied load the plate deflection at its centre increases, Fig. 5 (b) due to degraded stiffness properties. In Figure 5(b) the central deflection of the undamaged and damaged circular plate for different applied loads is presented. The curves start to divert at a load of 7 kN and the difference between the curves becomes significant at higher loads due to introduced fibre damage.

The area under the force-deflection curve for the damaged plate can be correlated to impact energy by the following equation:

$$\text{Impact Energy}=\text{Work}$$
$$\Rightarrow \frac{1}{2}mv^2=\int F\delta d \tag{16}$$

Figure 6 shows the quasi-static response obtained from the present model using the damage accumulation process described earlier (Eq. (15)) and compared to the quasi-static and impact test results. The peak contact force is plotted as a function of impact energy; the energy absorbed being calculated by integrating the area under the load-displacement curve, Fig. 5(b) on the basis of Eq. (16). It can be seen that at a given energy the analytically predicted peak force is in good agreement the measured static and impact test results.

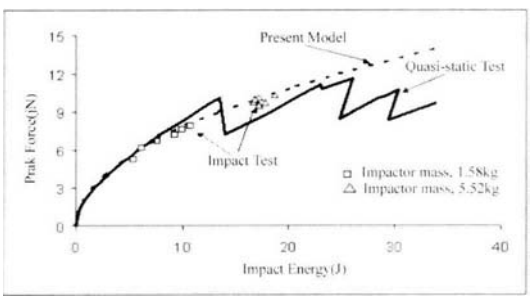

Fig. 6 Peak contact force against impact energy, predicted and measured values, for clamped IM7/8552 $[45/-45/0/90]_{3s}$ circular plates of 102 mm diameter

4.4 Damage area comparison between model, FE and experimental results

The maximum fibre breakage lengths predicted from the present simple model and FE77 (nonlinear static and dynamic analyses) and measured from impact tests are plotted versus the peak force and impact energy in Fig. 7(a) and (b), respectively. From these figures, the peak force and energy required to initiate fibre breakage can be obtained, namely 7 kN and 8 J from the simple analysis, 9 kN and 14 J from the nonlinear static FE analysis, 6.2 kN and 5 J from the nonlinear dynamic FE analysis and 9.7 kN and 17.8 J from the impact test. The fibre breakage length predicted from the present model is sharply increased after an applied load of about 14 kN, resulting in significant discrepancy between the model and the FE77 results. This is caused by the onset of fibre

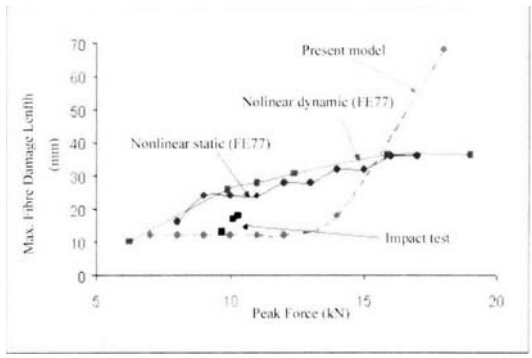

(a) Fibre damage length versus peak force

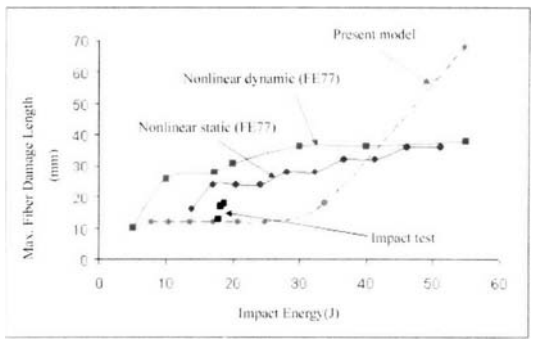

(b) Fibre damage length versus impact energy

Fig. 7 Impact damage in an IM7/8552 [45/−45/0/90]3s circular plate

damage caused by the membrane stretching effect, Fig. 5(a). The predicted fibre breakage lengths from the finite element analyses are in good agreement. The limited impact test results agree reasonably well with the theory but further testing is required.

5. Discussion

During impact, the damage of a plate consists mainly of transverse cracking, delamination, and fibre breakage due to both a concentrated force that induces high through-thickness stresses and large deflections, which induce bending and membrane stretching when the deflection exceeds the plate thickness. The current model only takes into account fibre breakage. Fibre breakage lengths were predicted successfully at each ply based on the maximum strain failure criterion. The predicted fibre damage lengths are in reasonable agreement with the numerical results (FE77) and impact test results.

From the results of the failure patterns of the 3 mm thick circular plates calculated from the present model, it is identified that damage is initiated from the plate centre but then as the load is increased a new damage area initiates which forms an annulus. The inner and outer damage ring increase in area as the load increases, Fig. 5 (a). All these failure patterns can be explained by the amount that the plate deflects due to lateral applied load. The non-linear strain equation, Eq. (14), consists of a membrane stretching strain term and a bending strain term. The bending strain term is important in the linear case where the plate deflection does not exceed the plate thickness. In the 3 mm thick plate with an initial damage load of 7 kN the deflection is 2.616 mm, which does not exceed the plate thickness and the overall strain is due to bending (linear case). As the applied load increases the plate deflection becomes larger than the plate thickness and the total strain is dominated by the membrane strain component (stretching). This is similar to the behaviour of the 1 mm thin plate where at a load of 10.5 kN extensive local damage occurs and the deflection of 6.175mm exceeds the plate thickness by more than six times. The membrane stretching effect, Fig. 8(a), dominates the overall nonlinear strain. In Fig. 8(a) radial bending strain distribution, radial membrane strain distribution and total radial strain distribution are plotted against the plate radius (a=51 mm) developed in the top and bottom plies when the applied load is 11 kN. Significant tensile strains due to stretching are developed in the top ply further away from its centre that can introduce significant tensile fibre breakage.

For a plate that is laterally deformed the deflection is inversely proportional to bending stiffness (bending stiffness rapidly increases because it is a function of t^3 where t is the plate thickness)). Figure 8(b) illustrates the radial strain distributions along the radius (a=51 mm) at the top and bottom plies of the 3 mm thick plate at an applied load of 8 kN. Figure 8(b) indicates that the bending strains are quite significant around

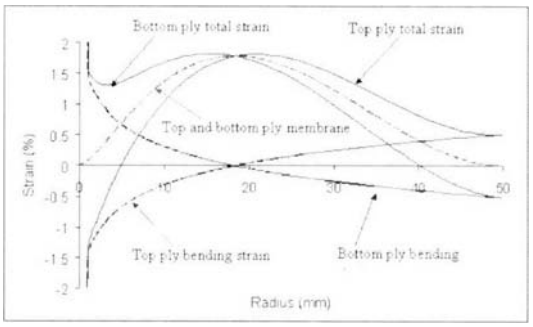

(a) 1 mm thick circular plate, applied load 11 kN

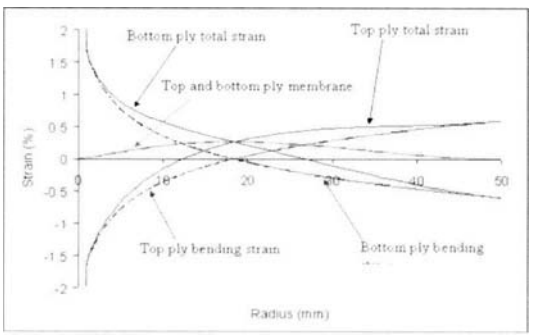

(b) 3 mm thick circular plate, applied load 8 kN

Fig. 8 Radial strain distributions along radius r at the top and bottom ply of the 1 mm thick circular plate (a) and 3 mm thick circular plate (b)

the central region while membrane strains are relatively small. The stretching effect get bigger at higher loads, Fig. 4(a), causing tensile damage in the form of fibre breakage away from the centre (17−20 mm).

It appears that the current analytical solution can save significant time in predicting the deformation and fibre damage area in composite plates under low velocity impact, compared with numerical solutions (FE). The deflection of the circular plate shown in Fig. 5(b) was calculated by the current model in five seconds compared to 120 minutes taken by nonlinear FE static analysis and 2460 minutes for the nonlinear FE dynamic analysis.

6. Conclusions

In order to predict the number of failed plies and the total fibre damage area introduced in an axisymmetric composite circular plate by a transverse load at its centre, an analytical model was developed using a simple non-linear approximation method (Rayleigh-Ritz method) and the principle of virtual work. As a failure prediction strategy for examining the fibre damage at each ply, the maximum strain failure criterion was adopted together with the classical laminate plate theory.

The present model agrees well with the finite element analysis for the deflection of the undamaged elastic plate and predicts successfully the number of failed plies and damage area due to fibre breakage in the shape of a circle. From the theoretical analysis, fibre damage at each ply of the plate shows two types of failure patterns. When the plate is quite thin (1 mm thick in the current analysis), fibre damage was produced by the effect of geometrical non-linearity, i.e. membrane stretching effect due to large deflection and the maximum non-linear effect occurred at a certain inner region of each ply displaying an overall annular damage shape. For a thick circular plate (3 mm thick), fibre damage initiated from the centre of each ply and propagated to the plate edge. In this case, the damage was dominated by bending effect since the plate deflection did not exceed the plate thickness. However, at a larger applied load, when the lateral deflection exceeded the plate thickness, fibre damage started to initiate at a certain inner region from the top ply like the case of the 1mm thick plate. Based on the number of failed plies in the plate, degraded elastic moduli were obtained using the classic laminate plate theory and the overall damage area was estimated. This could be used with a fracture mechanics based model (Soutis, 1995) to predict the compressive after impact (CAI) strength of any symmetric composite laminate. In addition, the simplified model presented here can save significant running time, compared with FE nonlinear static or dynamic solutions.

Acknowledgments

This work was carried with the financial support of the Structural Materials Centre, QinetiQ, Farnborough, UK. The authors are grateful for many useful discussions with Professor G.A.O. Davies of the Department of Aeronautics, Imperial College London, UK.

References

Chang, F. K. and Chang, K. Y., 1987, "A Progressive Damage Model for Laminated Composites Containing Stress Concentrations," *Journal of Composite Materials*, Vol. 21, pp. 834~854.

Davies, G. A. O. and Zhang, X., 1995, "Impact Damage Prediction in Carbon Composite Structures," *International Journal of Impact Engineering*, Vol. 16, No. 1, pp. 149~170.

Fuoss, E., Straznicky, P. V. and Poon, C., 1994, "Prediction of Impact □ Induced Delamination in Composite Plates," *Advanced Composite Letters*, Vol. 3, No. 3, pp. 193~196.

Fuoss, E., Straznicky, P. V. and Poon, C., 1998, "Effects of Stacking Sequence on The Impact Resistance in composite Laminates. Part 2: Prediction Method," *Composite Structures*, Vol. 41, No. 2, pp. 177~186.

Greszczuck, L. B., 1982, "Damage in Composite Panels due to Low Velocity Impact," Impact

Dynamics, Ed. Zukas Z.A. J. Wiley.

Hitchings, D., 1995, "FE77 User Manual Version 2.49," Imperial College, Aeronautics.

Khoo, S. W., 1991, "Low Velocity Impact of Composite Structures," Phd Thesis, University of London, December.

Kim, Y., Hwang, J., Baek, K., Cha, C. and Yang, I., 2003, "Impact Collapse Characteristics of CF/Epoxy Composite Tubes for Light-Weights," *KSME International Journal*, Vol. 17, No. 1, pp. 48~56.

Lee, J., 2003, "Compressive Behaviour of Composite Laminates before and after Low Velocity Impact," PhD Thesis, Imperial College London, UK..

Lee, S. R. and Sun, C. T., 1995, "On The Apparent Bending Isotropy in Clamped Elliptic Composite Laminates," *Journal of Composite Materials*, Vol. 29, No. 12, pp. 1601~1620.

Liou, W. J., Tseng, C. I. and Chao, L. P., 1996, "Stress Analysis of Laminated E-glass Epoxy composite Plates Subject to Impact Dynamic Loading," *Computers & Structures*, Vol. 61, No. 1, pp. 1~11.

Liu, D., 1988, "Impact-induced Delamination □ A View of Bending Stiffness Mismatching," *Journal of Composite Materials*, Vol. 22, pp. 674~692.

Monagan, M. B., 2000, "Maple 6: Programming Guide," Waterloo, Ont., Waterloo Maple.

Murri, G. B. and Guynn, E. G., 1988, "Analysis of Delamination Growth from Matrix Cracks in Laminates Subjected to Bending Loads," *Composite materials : Testing and Design (Eighth Conference)*, ASTM STP 972, pp. 322~339.

Sjobolm, P. O., Hartness, J. T. and Cordell, T. M., 1988, "On Low Velocity Impact Testing of Composite Materials," *Journal of Composite Materials*, Vol. 22, pp. 30~52.

Soutis, C. and Fleck, N. A., 1990, "Static Compression Failure of Carbon Fibre T800/924C Composite Plate with a Single Hole," *Journal of Composite Materials*, Vol. 24, pp. 536~558.

Soutis, C. and Curtis, P. T., 1995, "Prediction of The Post-Impact Compressive Strength of CFRP Laminated Composites," DRA/SMC Tech. Report. 951012. Nov..

Suemasu, H. and Majima, O., 1996, "Multiple Delaminations and Their Severity in Circular Axisymmetric Plates Subjected to Transverse Loading," *Journal of Composite Materials*, Vol. 30, No. 4, pp. 441~453.

Suemasu, H. and Majima, O., 1998, "Multiple Delaminations and Their Severity in Nonlinear Circular Plates Subjected to Concentrated Loading," *Journal of Composite Materials*, Vol. 32, No. 2, pp. 123~140.

Timoshenko and Woinowsky-Krieger, 1959, "Theory of Plates and Shells," McGraw-Hill Book Company, 2nd Ed..

Watson, S. A., 1994, "The Modelling of Impact Damage in Kevlar-Reinforced Epoxy Composite Structures," PhD Thesis, University of London, November.

Whitehead, R. S., 1985, "ICAF National Review," Pisa., pp. 10~26.